Summer 2024

High-Pressure Infiltration Process for Additively Manufactured Ceramic Matrix Composites

Samuel Weiler
Missouri University of Science and Technology

Department:

HIGH-PRESSURE INFILTRATION PROCESS FOR ADDITIVELY MANUFACTURED CERAMIC MATRIX COMPOSITES

by

SAMUEL BRANDT WEILER

A THESIS

Presented to the Graduate Faculty of the

MISSOURI UNIVERSITY OF SCIENCE AND TECHNOLOGY

In Partial Fulfillment of the Requirements for the Degree

MASTER OF SCIENCE IN MECHANICAL ENGINEERING

2023

Approved by:

Dr. K. Chandrashekhara, Advisor
Dr. Jeremy Watts
Dr. Jillian Schmidt

ABSTRACT

Ceramic matrix composites were developed in order to increase the fracture toughness, thermal shock resistance, and elongation of ceramic materials, while maintaining the very high temperature capabilities of these materials. A renewed focus has been placed on ceramic matrix composites due to the need for materials that maintain good mechanical strength at very high temperatures, for use in the extreme environments encountered by hypersonic vehicles, jet turbine blades, and the like. However, conventional methods to manufacture CMCs are costly and time consuming. The aim of this work is to develop a method for creating additively manufactured ceramic matrix composites using a high-pressure re-infiltration process. Samples were fabricated using a traditional resin transfer molding technique, as well as the new high-pressure system developed for this work. For both techniques, AM carbon fiber/PEEK composite parts were used for the composite preform, and SC-1008 phenolic resin was used as the ceramic precursor. Pyrolysis cycles were performed between infiltration stages to convert the phenolic resin into the desired carbon matrix. The two techniques were compared to each other, analyzing the latent porosity resulting from each technique, and the resulting microstructure of the composite was examined. The high-pressure re-infiltration system developed in this work had less latent porosity after pyrolysis stages, and required fewer re-infiltration and pyrolysis cycles in order to achieve a desired porosity. These results suggest that a high-pressure re-infiltration technique could be used to create carbon/carbon CMCs faster and cheaper than traditional techniques.

ACKNOWLEDGMENTS

I would like to thank Dr. K. Chandrashekhara for his continuous guidance and advice throughout my higher education journey. Dr. Chandrashekhara consistently pushed and encouraged me throughout my educational career. I also wish to thank my committee members Dr. Jeremy Watts, and Dr. Jillian Schmidt. Special thanks goes to Dr. Greg Hilmas, Dr. Manoj Rangapuram, Dr. Krishna Darasi, Henry Haffner, Nayan Pundhir and all the other students of my research team, for their support, insight, and experience, which they graciously shared.

Support and expertise from Jeff DeGrange and Dr. John Bayldon at Impossible Objects and Dr. Lisa Rueschhoff at the Air Force Research Lab is gratefully acknowledged.

I would like to thank Ed and Carol Haug, the Missouri Space Grant Consortium, and the Chancellor's Scholarship for their financial support throughout my college education.

Finally, I would like to thank my mother, father, sisters, and all the other family and friends who supported me, encouraged me, and believed in me.

TABLE OF CONTENTS

Page

LIST OF ILLUSTRATIONS

Page

LIST OF TABLES

Page

1. INTRODUCTION

With advances in hypersonic aeronautics, jet engine technology, and other industries, the need for very high temperature, high strength materials has grown rapidly in previous years [1,2]. While uses for these materials are still being found, engineers have developed a general set of requirements that many of the potential uses need to possess. For a material to be successful in these industries, they need to be stable at high temperatures (above 1000°C), they need to possess high thermal shock resistance, as they may experience rapid heating and cooling cycles, and they need to be lightweight for use in aircraft [3]. These materials should also be highly resistant to crack propagation. In order to meet these requirements, engineers have suggested the use of ceramic matrix composites [4].

1.1. CERAMIC MATRIX COMPOSITES

Due to the strict requirements outlined above, engineers have turned to ceramic matrix composites (CMCs) for high temperature structural applications. Ceramic materials are inorganic, non-metallic materials that are typically shaped at room temperature, and require sintering at high temperatures in order to achieve their typical properties [5]. Typically, ceramic materials are characterized by good corrosion, wear, and heat resistance, as well as extreme hardness, and low electrical conductivity [6]. However, some of these characteristics, such as high hardness and low fracture toughness, are undesirable in many engineering applications [3]. In order to mitigate

these characteristics, without impacting the desirable characteristics, engineers have developed ceramic matrix composites.

Ceramic matrix composites are any composite materials that use a ceramic material as its matrix. By using a ceramic matrix, the composite maintains good corrosion and heat resistance, but reduces the brittleness to a more desirable range [3,7]. Typical techniques for manufacturing CMCs include liquid silicon infiltration (LSI), chemical vapor infiltration (CVI), and chemical vapor deposition (CVD) [8]. However, many of these techniques can result in high porosity, significantly reducing the material properties of the resultant composite [9,10]. These processes are also typically expensive and time consuming, potentially taking weeks to produce a part [11]. Polymer infiltration and pyrolysis (PIP) has shown promise as a method to produce low cost, highly dense CMCs without extensive lead times [10,11,12]. With adjustments to the PIP process such as the application of pressure during resin infiltration and the incorporation of additively manufactured composite preforms, it should be possible to reduce the residual porosity of CMC materials as well as reduce the amount of time needed to manufacture them.

1.2. STUDY OVERVIEW

The aim of this work is to develop a method of high-pressure polymer infiltration and pyrolysis to manufacture CMCs with a preceramic polymer precursor. Samples were produced with both the traditional PIP process, and the high-pressure PIP process that was developed. A comparison of the two materials was made in order to establish the advantages and disadvantages of each manufacturing method.

2. MATERIALS

2.1. SELECTION

The materials for this project were selected with the goal of producing high quality, dense CMCs with randomly oriented or woven long fibers. SC-1008 phenolic resin was chosen as the ceramic precursor due to its commercial availability, high char yield, and ease of use from its ability to be used for room temperature infiltration processes [13]. Additively manufactured composites were used as fiber reinforcement, due to their fast manufacturing time, and ability to make shaped CMCs [14,15]. The aim of this work, however, is to develop a general manufacturing process to produce CMCs, and it can be applied to many combinations of fiber reinforcement and preceramic polymer matrix. The materials were consistent throughout the work in order to focus only on the differences that result from the manufacturing process, not the differences from using different material systems.

2.2. CERAMIC PRECURSOR

A ceramic precursor is a polymer compound that, though pyrolysis under controlled conditions, is converted into a ceramic material [16]. There are a wide variety of ceramic precursors, such as amorphous silicon carbide (SiC), silicon oxycarbide (SiOC), silicon carbonitride (SiCN), and phenol-formaldehyde (phenolic) resins [17]. For this work, Durite™ SC-1008, a phenolic resole resin, was identified for its high char yield and ease of use in a VARTM process, due to its low viscosity at room temperature.

Phenolic resole resins are made with a formaldehyde to phenol ratio of greater than 1 (typically around 1.5) [18]. Because there is an excess of formaldehyde to phenol, each phenol is linked to a formaldehyde, and the entire system is crosslinked [19]. This means that resole phenolics can be cured without the addition of a curing agent. The SC-1008 resin used in this work has a two-stage cure cycle, shown in Figure 2.1, provided by the manufacturer.

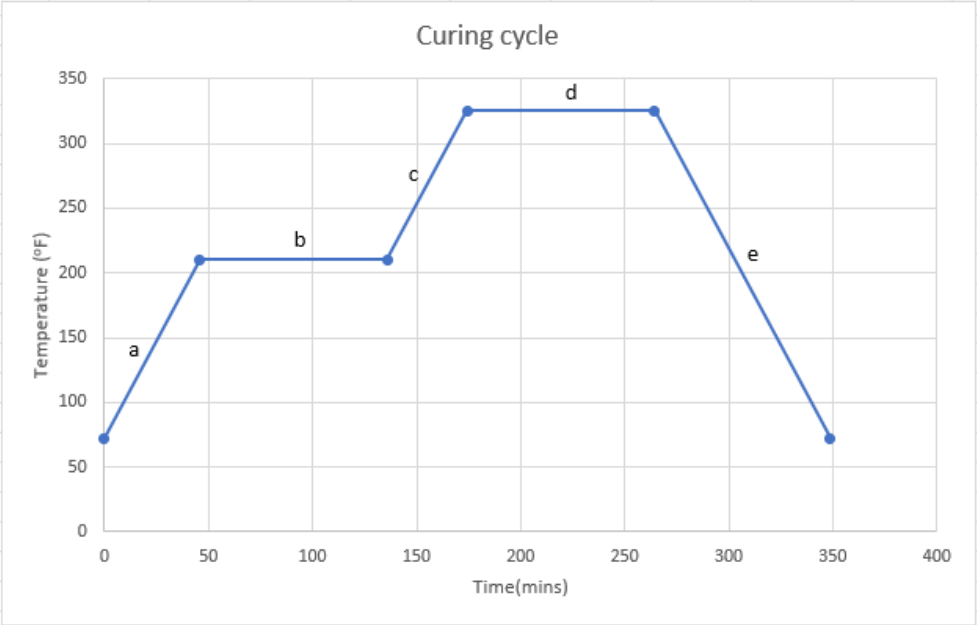

Figure 2.1 SC-1008 Cure Cycle

Where all the ramps (a, c, and e) are at 3ºF/min, and (b) and (d) are holds at 210ºF and 325ºF, respectively. The properties of the SC-1008 resin are shown in Table 2.1, as obtained by the Hexion Data Sheet [20].

In order to verify the curing cycle of the resin chosen for this work, as well as to better understand the properties of the resin, DSC/TGA was performed on a sample of the

SC-1008 resin. The result of this test is shown in Figure 2.2. The equipment used was a Netzsch STA 449 F5 Jupiter, with a heating rate of 5ºC/min to 1000ºC.

Table 2.1 Properties of SC-1008 Phenolic Resin

Property	**SC-1008**
Density (g/cm^3)	10.7 – 1.10
Appearance	Clear, Amber Liquid
Viscosity (cps at 25ºC)	180 - 300
Solids Content (%)	60 - 64
Char Yield (%)	55
Flash Point (ºC)	26.7

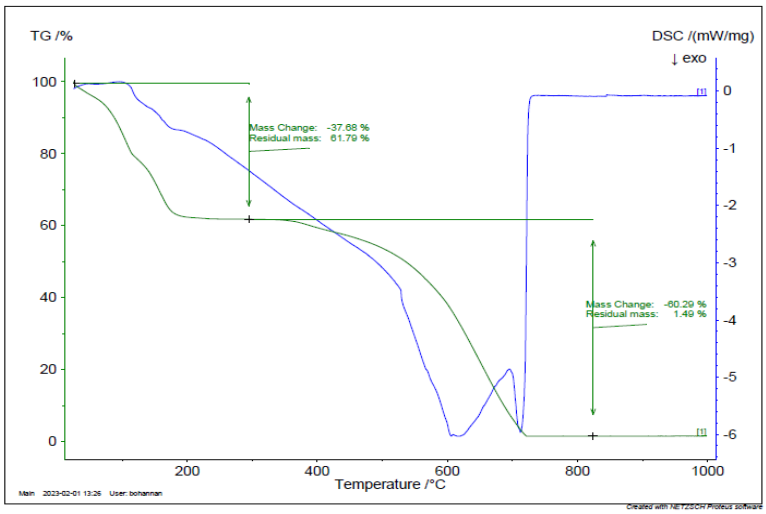

Figure 2.2 DSC/TGA Results for SC-1008

Analyzing the results of the DSC/TGA, there is a plateau at 61.79% residual mass, representing the fully cured state of the SC-1008, having driven off all the solvent.

This falls within the range of 60-64% solids content provided by the manufacturer of the resin.

2.3. FIBER REINFORCEMENT

The fiber reinforcement used in this work is a medium modulus carbon fiber, supplied by Impossible Objects (IO). This fiber is in the form of a randomly oriented long fiber mat, used in the CBAM 2 machine, manufactured by IO in Northbrook, IL.

Composite Based Additive Manufacturing (CBAM) is an additive manufacturing method for manufacturing composite components. The CBAM-2 machine utilizes inkjet binder technology to deposit a binder onto the composite sheets, then spreads a uniform layer of polymer powder over the entire sheet. The powder that does not come into contact with the binder is then vacuumed away and recycled for later sheets. The powdered sheets are stacked, and loaded into a hot press. The press is activated, compressing the stack, and melting the powder polymer. This heated pressing binds and consolidates the sheets into one dense composite part. Once cooled, the unbound fibers can be sandblasted away, revealing the completed part [21]. A schematic of this process can be seen in Figure 2.3.

The specifications for the CBAM-2 Printer can be seen below in Table 2.2 [21]. The CBAM-2 Printer is capable of printing with either fiberglass or carbon fibers, and either nylon or polyetheretherketone (PEEK) matrixes [22]. For this work, PEEK was used as the matrix material with carbon fiber sheets.

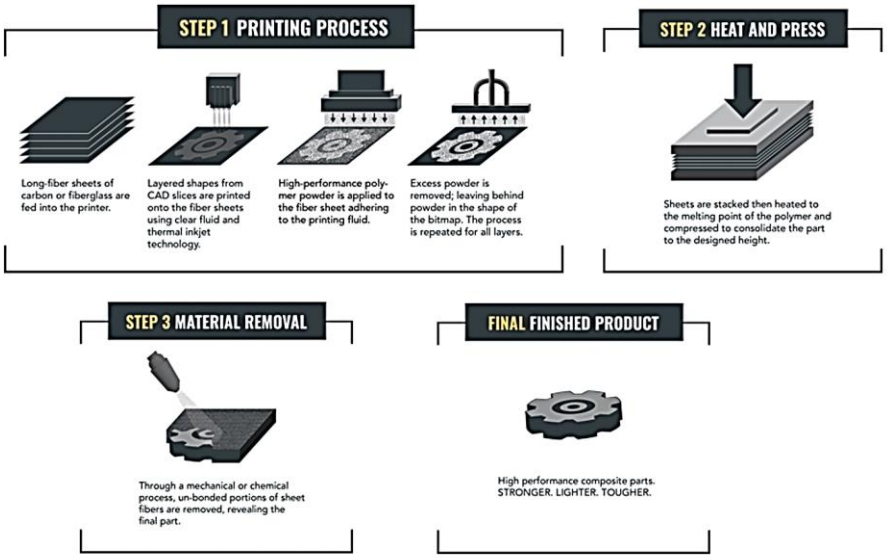

Figure 2.3 CBAM-2 Process Schematic

Table 2.2 CBAM-2 Specifications

Specification	**CBAM-2 Printer**
Speed (in^3/hour)	45
Build Volume Dimensions (in)	12 x 12 x 4
Print Resolution (DPI)	600
Accuracy (%)	0.1
Layer Height (in)	0.002

3. MANUFACTURING

3.1. OUTLINE

Two manufacturing processes were investigated for this work. A traditional out of autoclave (OOA) vacuum infusion technique, as well as a high-pressure injection technique were used to manufacture the samples. An OOA technique uses only atmospheric pressure to cure the resin [23,24]. The samples were pyrolyzed and re-infiltrated, measuring the porosity at each stage of the process, in order to determine the change in porosity throughout the manufacturing of CMCs.

3.2. PYROLYSIS PROCESS

After initial manufacture using the CBAM-2 machine, as well as after each re-infiltration cycle, the samples went through pyrolysis to create the ceramic matrix. Pyrolysis is the high temperature firing of a material in order to change its chemical composition [25]. In this case, the SC-1008 is converted into carbon during pyrolysis [26]. The pyrolysis schedule is outlined below in Figure 3.1. The sample is heated to 60°C/min to 100°C, then at 5°C/hr to 500°C. The oven is held at that temperature for 2 hours and then cooled to room temperature. In order to prevent expansion of the samples during pyrolysis, the samples are placed between a porous alumina setter which takes up the extra space in the oven and limits expansion. The entire process takes approximately 4-5 days to complete.

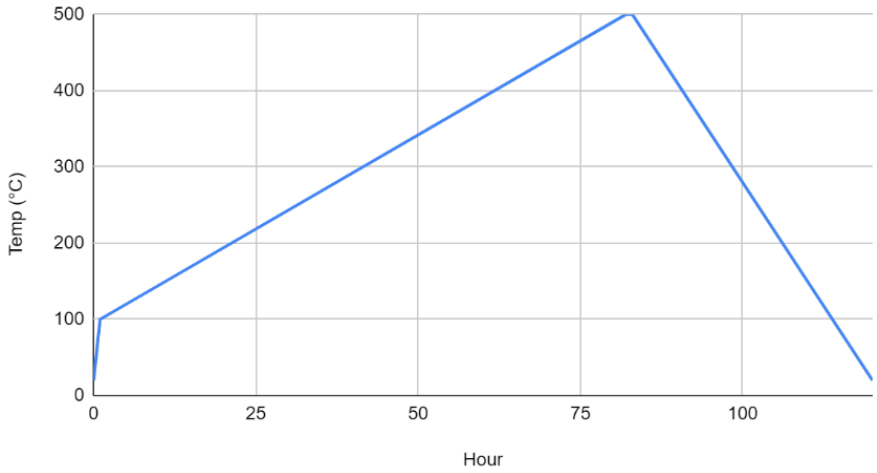

Figure 3.1 Pyrolysis Schedule

3.3. LOW-PRESSURE VACUUM ASSISTED RESIN TRANSFER MOLDING PROCESS

Before beginning the high-pressure resin injection process, samples were manufactured with a low-pressure infusion process. This provides a baseline to compare the high-pressure infiltration process and serves to provide a fundamental understanding of the process. The low-pressure system utilized for this work is vacuum assisted resin transfer molding (VARTM).

Vacuum assisted resin transfer molding is an out of autoclave, closed mold technique of resin transfer molding that uses vacuum pressure to aid in the infusion of the fibers. A schematic of this process can be seen in Figure 3.2. This process was chosen to serve as the baseline because of its low tooling cost, as only one side of the mold is a hard tooling surface, while the other side is a vacuum bag [27]. Other benefits of this process include a short start-up time and high adaptivity to various shapes and material systems [28].

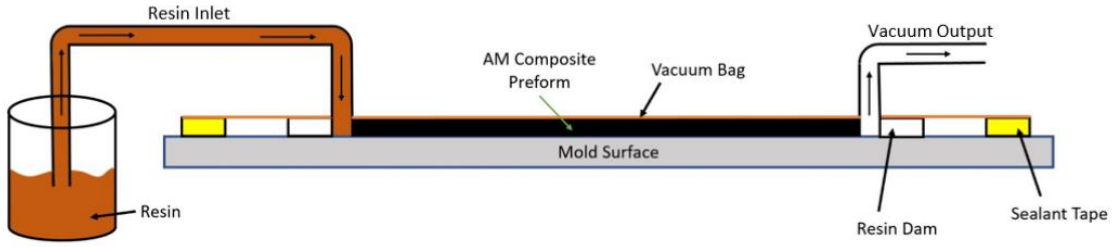

Figure 3.2 Schematic of the VARTM Process

In the VARTM process, the part is placed onto either a flat or contoured mold surface. The mold can be coated with a sealing agent and a release film in order to prevent the part sticking to the mold when removing. Teflon release film is added to the top of the part to prevent sticking to the vacuum bag, as well as prevent puncturing the vacuum bag on any sharp corners. A porous flow medium is added to aid in the flow of air out of the mold and resin into the mold. Finally, a vacuum bag is added, sealed with sealant tape around the edges. Two tubes are set in place, one acting as a resin inlet and the other as the vacuum outlet. The vacuum is activated, evacuating air out from the mold. The resin inlet is opened, allowing the resin to flow into the mold. The system remains under vacuum until the infiltration is complete, between 30 to 60 minutes, or more. Finally, the resin inlet can be closed, and the part can be placed into an oven to cure. This process in progress can be seen in Figure 3.3.

Samples were manufactured using a carbon fiber mat and a PEEK matrix using IO's CBAM 2 machine. After manufacture, the samples were pyrolyzed to burn away the PEEK matrix. The parts are then re-infiltrated using the above process, with Hexion SC-1008 phenolic resin. The process of pyrolyzing and re-infiltrating the samples can be repeated until the desired porosity is reached. For this work, smaller samples were taken

from the main sample after each stage of the process, for later analysis. An image of a sample after infusion can be seen in Figure 3.4.

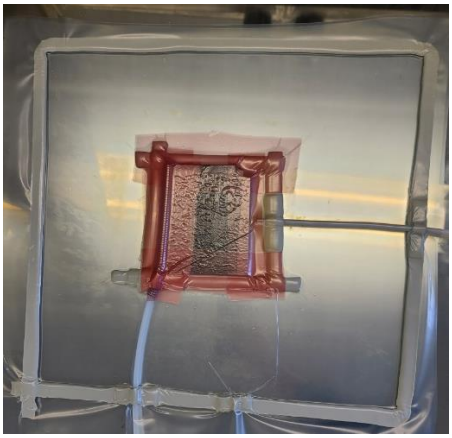

Figure 3.3 VARTM Process in Progress

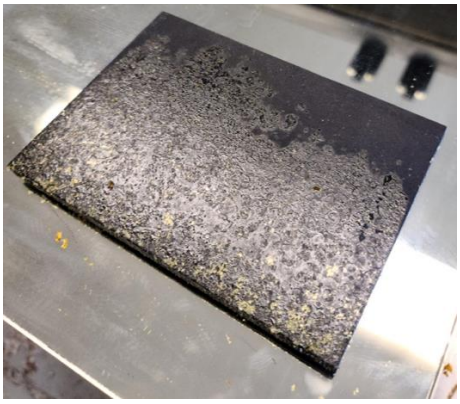

Figure 3.4 Sample after Low-Pressure Re-Infiltration

3.4. HIGH-PRESSURE RESIN INJECTION PROCESS

It was theorized that by using a high-pressure resin injection process, the number of re-infiltration and pyrolysis cycles required to reach a desired porosity is minimized.

By maximizing the pressure differential between the resin inlet and outlet, the time to infuse the resin and the latent porosity after infusion can be reduced.

3.4.1. Overview. Fundamentally, the process for high-pressure resin injection is much the same as low-pressure infusion. The high-pressure setup has two sections; the control unit, and the mold side. The control unit houses the resin inlet line, the actuation and pressurization pistons, and the controls for the entire system. The mold side includes the mold, a table to securely mount it, and the resin inlet and vacuum outlet. The entire setup is shown below, with each component labeled, in Figure 3.5.

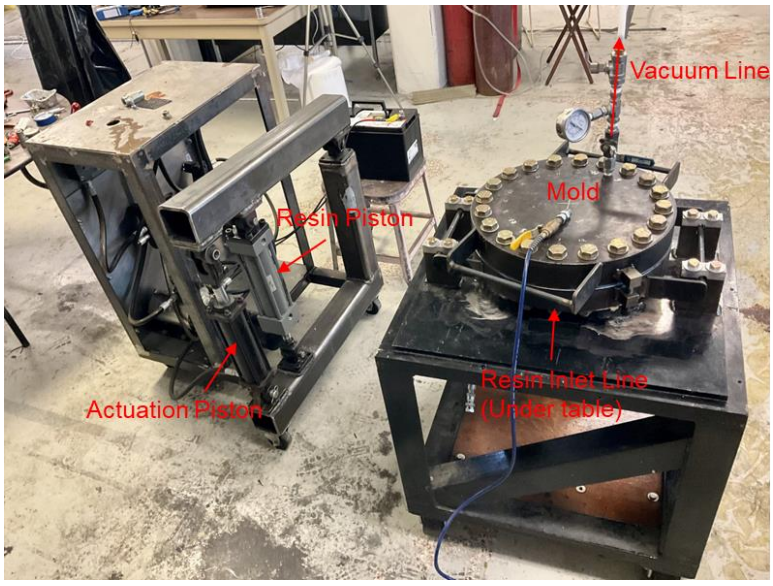

Figure 3.5 High-Pressure Infiltration Setup

Instead of using a vacuum bag, the part is placed in a steel mold, detailed below in Section 3.4.2. The mold has vacuum outlet and resin inlet lines built into the mold surfaces. The mold is prepared with a sealant agent and release agent prior to use. Once the mold is loaded with the fiber preform and sealed, the vacuum can be activated, and air

evacuated from the mold. The resin inlet line can then be opened, pulling resin into the resin pressurization cylinder and the mold via vacuum pressure. Once the resin fills the system and reaches the vacuum line, the vacuum is turned off, and the resin inlet is closed. This seals both gates into and out of the system. The actuation piston can now be activated, compressing the resin piston and pressurizing the resin. A pressure gauge on the mold provides a read out of the current resin pressure. Once the resin reaches the desired pressure, it is left to settle, as the resin fills any open porosity not previously infiltrated with resin. As this happens, a drop in pressure should be observed on the pressure gauge. A “bump” of the resin pressure may be required to re-pressurize the resin to the desired pressure. Once the pressure remains relatively constant, valves can be closed, isolating the mold from the rest of the system. The resin inlet and vacuum outlet lines can be disconnected, and the mold and mold table transferred to an oven. The resin can be cured using the cure cycle in Figure 2.1. Once cured, the mold is allowed to cool to handling temperature, and the mold can be opened to the finished part. It is important to clean all parts of the system that were in contact with resin with a non-water based cleaner and protectant. This system has been successfully tested with high-pressure injection tests to 1000 psi. Figure 3.6 below shows a high-pressure sample before and after re-infiltration.

3.4.2. Mold Design. A custom AISI 1054 medium carbon steel mold was fabricated for this work. The mold is built to withstand a resin pressure of 1500 psi, and features O-rings to prevent resin leakage, as well as 20 bolts to provide the required clamping pressure. The mold can produce parts of up to 11” in diameter, with the shape being determined by the design of the mold spacer, outlined below in Section 3.4.3.

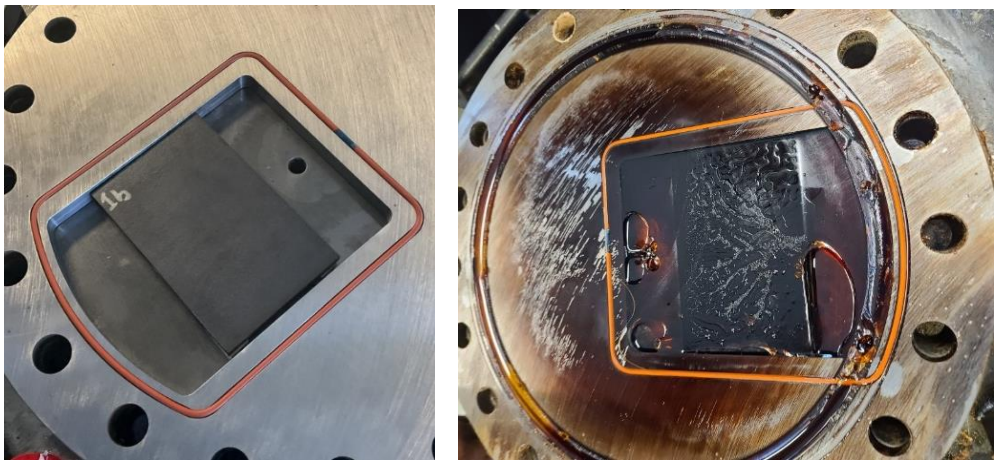

a b

Figure 3.6 High-Pressure Sample a) before and b) after re-infiltration

The assembled mold weighs 325 lbs, and proper personal protective equipment should be worn when working with the high-pressure re-infiltration setup. An image of the two mold halves, as well as the space is shown below in Figure 3.7. The CAD drawing of the top place is shown in Figure 3.8.

Figure 3.7 High-Pressure Injection Mold (Top Plate, Spacer, and O-rings on left; Bottom Plate on Right)

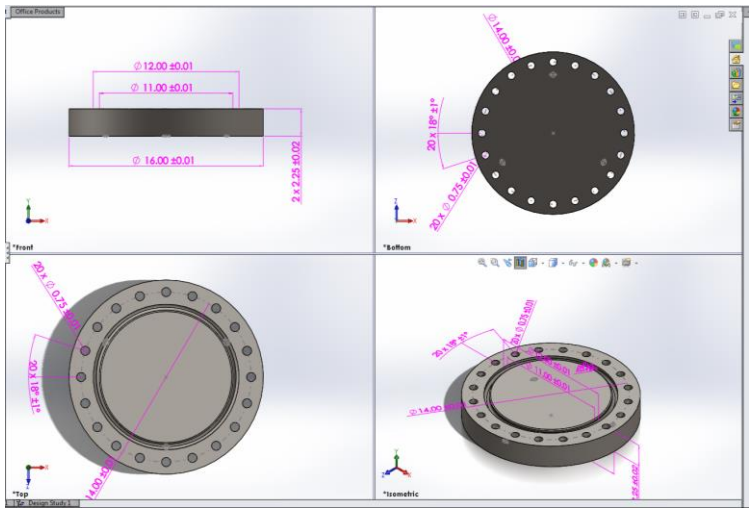

Figure 3.8 Top Plate CAD (Dimensions in Inches)

The resin inlet line is attached to the bottom plate of the mold, in the center of the cavity. The vacuum outlet line is a circular grove around the circumference of the cavity. This creates a pressure gradient between the center of the mold and the edges, causing the resin to flow radially. A groove for the O-ring creates a seal between the top plate and the spacer, and the spacer and the bottom plate.

Once the preform is loaded into the mold, the mold can be sealed. The sealing process involves tightening 20 SAE grade 8, ¾-16 bolts in three stages. In order to prevent binding caused by the clamping force of the bolts, the tightening pattern shown in Figure 3.9 should be utilized.

In order to reach the required clamping force, each bolt should be tightened to a torque of 320 lb. ft. To prevent binding, the bolts should be tightened in 3 stages, increasing the torque by 1/3 of the required in each stage.

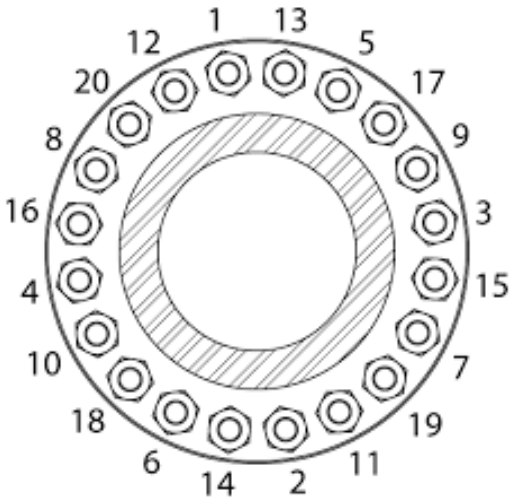

Figure 3.9 Pattern for Tightening Bolts

The mold also features five ball valves, each used to direct flow to certain areas, or maintain pressure in the mold. The valves are the resin inlet valve, the purge line valve, two mold isolation valves, and the vacuum outlet valve. By opening and closing certain valves at different stages of the process, the pressure can be safely controlled, and resin can be directed into the mold cavity, excess resin drained out, and the mold isolated from the rest of the system while under pressure, in order to be moved into an oven for curing.

The re-infiltration process begins by closing all the valves, and expanding the resin cylinder to approximately 75% open. Opening all valves except for the purge line valve, and the resin inlet valve, and turning on the vacuum pump starts the process of evacuating air out of the system. When the vacuum gauge reads sufficient vacuum pressure, the resin inlet valve can be opened, pulling resin into the mold by vacuum pressure. Once the mold and resin cylinder are filled and resin is visible in the vacuum line, the vacuum outlet line and resin inlet line can be closed, sealing the resin into the

system. The actuation piston can then be activated, compressing the resin and pressurizing it. Once the desired resin pressure is reached, the actuation piston is stopped, and the pressure is monitored. A drop in pressure is typical, as the resin flows into porosity in the part. Additional pressure increases may be required, until the pressure remains steady after pressurizing. The part is considered fully infiltrated at this point, and ready to cure.

The mold isolation valves on the top and bottom faces of the mold can be closed, sealing the mold cavity and the pressurized resin inside of it. The hoses are then disconnected, and the mold and mold table can be placed into an oven. The sample is cured using the cure cycle in Figure 2.1. Once the mold has cooled to room temperature, it can be removed from the oven and opened. The bolts are loosened using the same process as tightening them, but in reverse. There is a pultrusion on both mold plates, with a screw that can be tightened to break the seal between the two halves. Once opened, the cured part can be carefully removed from the mold.

3.4.3. Mold Spacer Design. The shape of the part produced using the high-pressure re-infiltration system is determined by the shape of the spacer used between the two mold halves. The mold spacer can be any number of shapes, but there are currently two spacers in use. The first is the simplest, shown above in Figure 3.7. It is made from a 0.25” steel plate, with an 11” diameter circle cut from it and 20 holes spaced for the bolts to hold it together. The inner circle is wide enough to clear the opening for the vacuum outlet line, maintaining the radial resin flow configuration present in the mold halves. This spacer creates a part that is 0.25” thick and 11” in diameter.

The second mold spacer in use is purpose built for the samples being used in this work. The spacer design is shown in Figure 3.10. The sample size chosen for this work is 3.5” by 5”, and nominally 4mm thick. The cavity in the spacer is sized to fit the samples and minimize resin waste due to excessive space. The spacer is manufactured from 0.5” steel, in order to account for the variability in sample thickness after pyrolysis. The cavity is also situated to provide a clear path for resin flow, from the center of the mold to an edge, creating a linear flow front. The spacer also features a groove on the top and bottom surfaces, offset from the edge of the cavity, in order to seat an O-ring and prevent resin leaking from the mold.

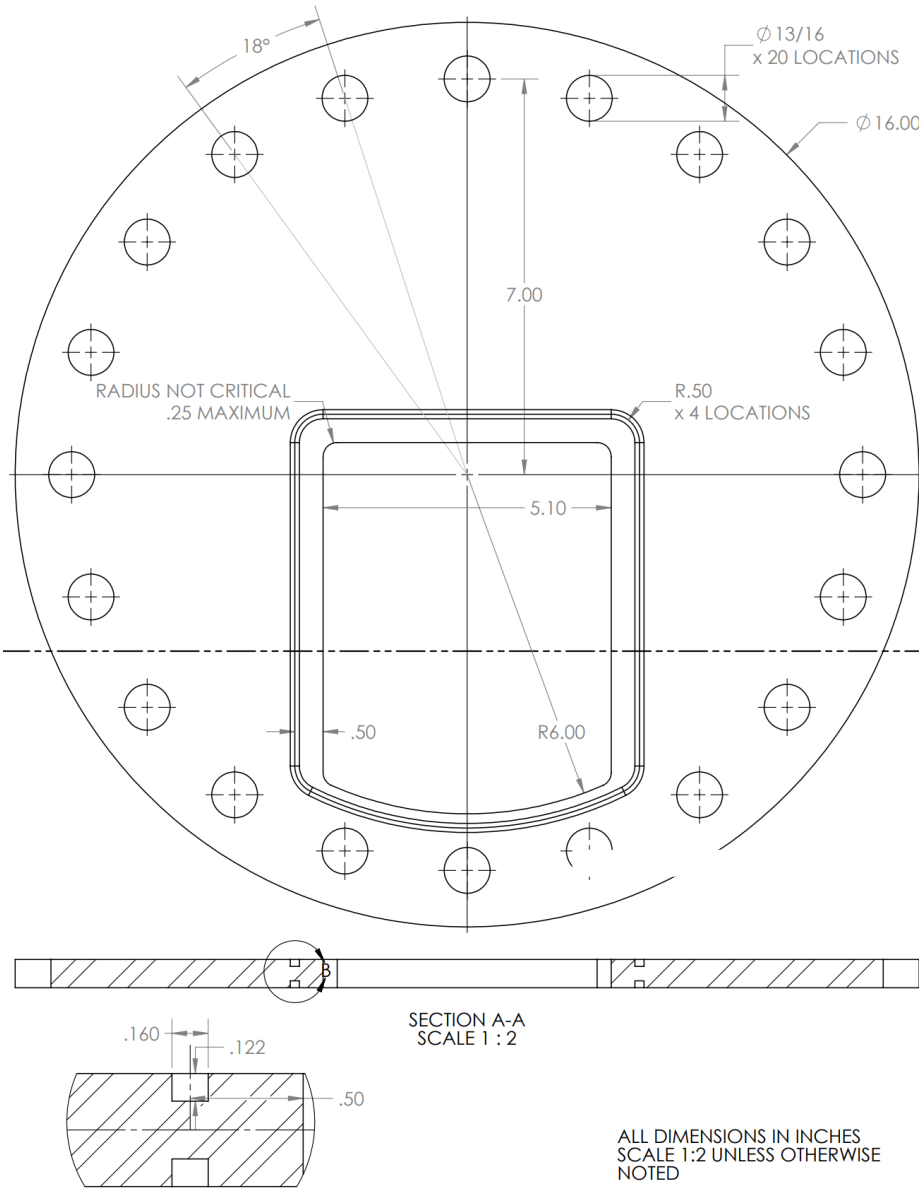

Figure 3.10 Mold Spacer Design

4. POROSITY ANALYSIS

One of the most important characteristics of the materials produced at this stage of the work is the latent open porosity of the part after pyrolysis. This represents the amount of porosity in the part, after the resin has been pyrolyzed and converted into ceramic. This property has a large impact on the performance of the material, and for the goals of this work, less porosity after pyrolysis is better. Porosity measurements were taken at each stage of the manufacturing process, in order to model the porosity change as the samples are manufactured. Open porosity is preferred over closed porosity, as open porosity remains accessible to resin infiltration during subsequent re-infiltration cycles. It would not be possible to fill the closed porosity without an additional step in the manufacturing process to convert that porosity to open porosity. Porosity was measured using Archimedes' Principle of fluid saturation.

4.1. ARCHIMEDES POROSITY

In order to determine the porosity using Archimedes' Principle of fluid saturation, small samples are taken from the larger samples after each re-infiltration and pyrolysis stage. The weight of each sample is taken and recorded. The samples are submerged in water, weighing them down if necessary, and placed in a vacuum chamber. The vacuum is activated, and the sample is left in the chamber for 24 hours. This process pulls any air out of the porosity in the sample. When the vacuum pump is deactivated, air reenters the chamber, increasing the pressure. This pressure forces water into the porosity of the sample, replacing the air in the pores. The sample is removed from the vacuum chamber,

and placed on a basket in another beaker of water, on a scale. This weight is denoted as the suspended weight. The sample is then removed from the beaker, and the exterior of the sample is dried with a damp paper towel. Care should be taken to not over dry the sample, as only the surface of the sample should be dried, without pulling any water out of the pores of the sample. Once dried, the sample is placed in a basket above the beaker, also on the scale, and the weight taken. This weight is denoted as the saturated, or wet, weight. An image of the setup is shown in Figure 4.1.

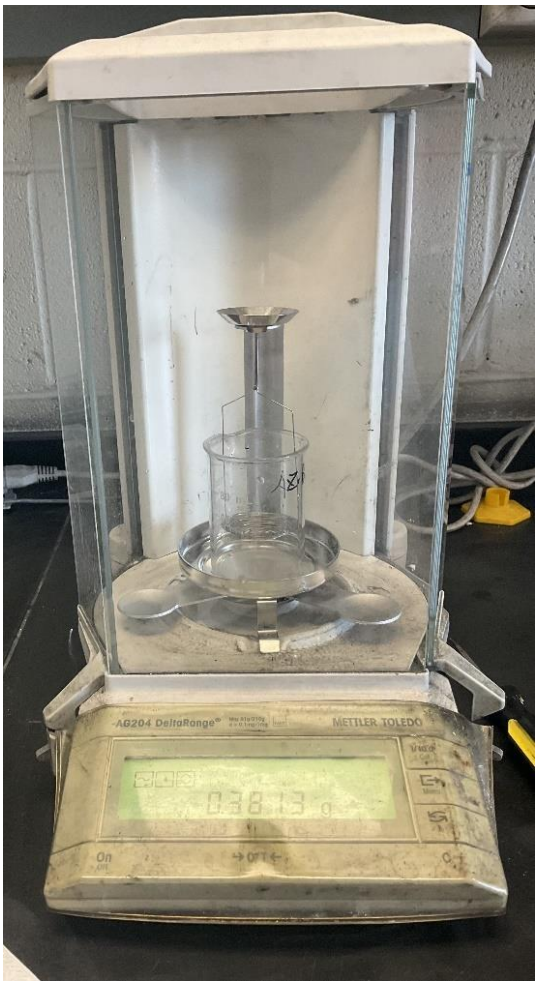

Figure 4.1 Archimedes' Principle of Fluid Saturation Setup

Using the following set of equations, density and open porosity can be calculated.

$$V_B = \frac{M_{sat} - M_{sus}}{\rho_w} \quad (1)$$

$$V_p = \frac{M_{sat} - M_{dry}}{\rho_w} \quad (2)$$

$$\phi = \frac{V_p}{V_B} \quad (3)$$

Where M_{sat}, M_{sus} and M_{dry} correspond to the saturated, suspended, and dry weights respectively, V_B and V_p correspond to the bulk volume and volume of open porosity, ρ_w is the density of water, and ϕ is the percent porosity.

Using the above equations, the porosity results can be calculated at each stage of re-infiltration and pyrolysis cycles. These results are tabulated and summarized in Section 6, Results and Discussion.

4.2. POROSITY MODELING

In order to better understand the process that drives the amount of latent porosity in a sample after re-infiltration and pyrolysis, a model for porosity was created. This model considers the initial porosity, the inaccessible volume, the solid content of the resin, and the char yield of the resin to predict the porosity after pyrolysis. The inaccessible volume is a term that combines all vole that cannot be filled with resin, either due to closed porosity, or from reasons related to the process. The model derived is shown below in Equation 4.

$$V_{rp} = V_i - (V_i - V_r)V_s C_v \quad (4)$$

Where V_i is the initial volume, V_r is the inaccessible volume, V_s is the solid content of the resin, C_v is the char yield of the resin, and V_{rp} is the porosity after pyrolysis.

This equation can be iterated in order to predict the porosity after a certain number of re-infiltration and pyrolysis stages, for varying resin properties and inaccessible volumes (process driven properties).

It was desired to analyze the model and determine which variables could be identified as the ones that drive the number of cycles to reach a certain porosity. Inaccessible volume and solid content are values that could reasonably be changed. The initial volume of porosity is, for the most part, constant based on the CBAM 2 machine. This value is approximately 60% after initial pyrolysis. The char yield of the resin is also held constant, as there is no easy way to raise this value without adding fillers or additives, that add significant complications to the process. Varying values of inaccessible volume and solid content were input into the model, and the model iterated. The solid contents used were 62%, the value of the resin as received, and 80%, an estimation of how much solvent could be removed before the resin is too viscous to be used in this process. Results of this iteration is shown in Figure 4.2. In the figure, solid lines denote a solid content of 62%, while dashed lines denote a solid content of 80%. Blue lines have an inaccessible volume of 35%, green is 10%, and red is 2% inaccessible volume.

Looking at the graph, it is clear that for each set of values, the porosity quickly drops off, before leveling off around the inaccessible volume value. Once the amount of

porosity nears the inaccessible volume, there is not a significant amount of resin infiltrating into the sample, and the volume remains constant. Also, for each set of values, there are diminishing returns from performing more re-infiltration and pyrolysis cycles. After about 5 cycles, most of the pores that are going to be filled have been. The solids content of the resin does impact the porosity of the samples after each stage, but it is not as significant as the impact of the inaccessible volume.

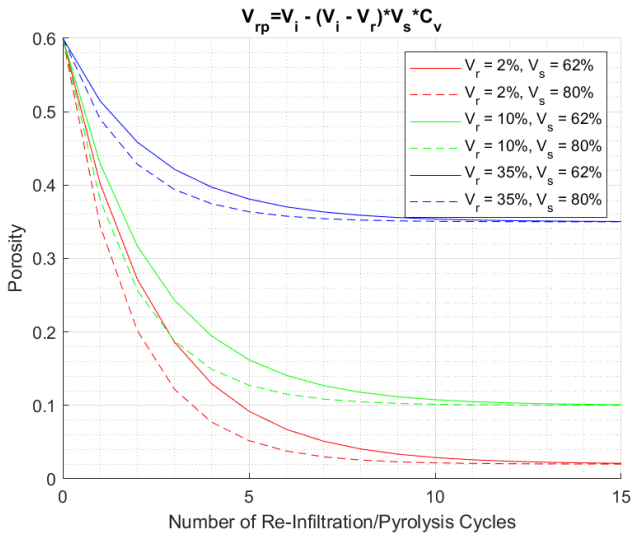

Figure 4.2 Porosity Modeling Study

This study was successful in providing a better understanding of what drives the porosity in the samples after re-infiltration and pyrolysis cycles. Identifying the driving factor of the porosity confirms the focus of this work, as minimizing the inaccessible volume is primarily a process driven problem. By pressurizing the resin during re-infiltration, it is theorized that the inaccessible volume will be decreased, as more resin is forced into the sample.

5. MICROSTRUCTURE ANALYSIS

Microstructural analysis allows for the investigation into the characteristics of the finished CMC part. The microstructure of a CMC greatly affects the material properties of the finished part. High void content or inconsistent matrix densities have a negative effect, where consistent matrix densities, good fiber wet-out and consolidation, and low porosity all suggest a material with better properties. Microstructural analysis also allows for the inspection of defects present in the part, and can provide insight in how to modify the process to limit those defects from forming.

5.1. OPTICAL MICROSCOPY

Due to its simplicity to perform and ability to produce color images, optical microscopy was used to initially study the microstructure of the parts. While the power of optical microscopy is limited compared to other methods like scanning electron microscopy, it is still able to provide valuable insight into the microstructure of the parts before and after resin infiltration.

All of the optical microscopy images for this work were taken on a ZM-4TZ3 AmScope Trinocular Stereo Microscope.

Optical microscopy images were taken at many points in the re-infiltration process, as a quick method to understand the behavior of the sample throughout the process. The following images were taken after the initial re-infiltration process. The sample has not been pyrolyzed, other than the initial pyrolysis to burn away the PEEK resin. Figure 5.1 below shows the sample after being removed from the vacuum bag. The

was an inconsistent surface finish visible on the top surface of the part, with more resin appearing to be deposited on the surface of the part closer to the resin inlet, and less resin on the surface nearest to the vacuum output. Because of this inconsistency, it was theorized that there may have been more resin deposited into the sample closer to the resin inlet, leading to inconsistent matrix density throughout the sample. Within Figure 5.1, a) was taken looking at the front edge of the sample, nearest the resin inlet, while b) was taken of the back edge of the sample, nearest the vacuum output.

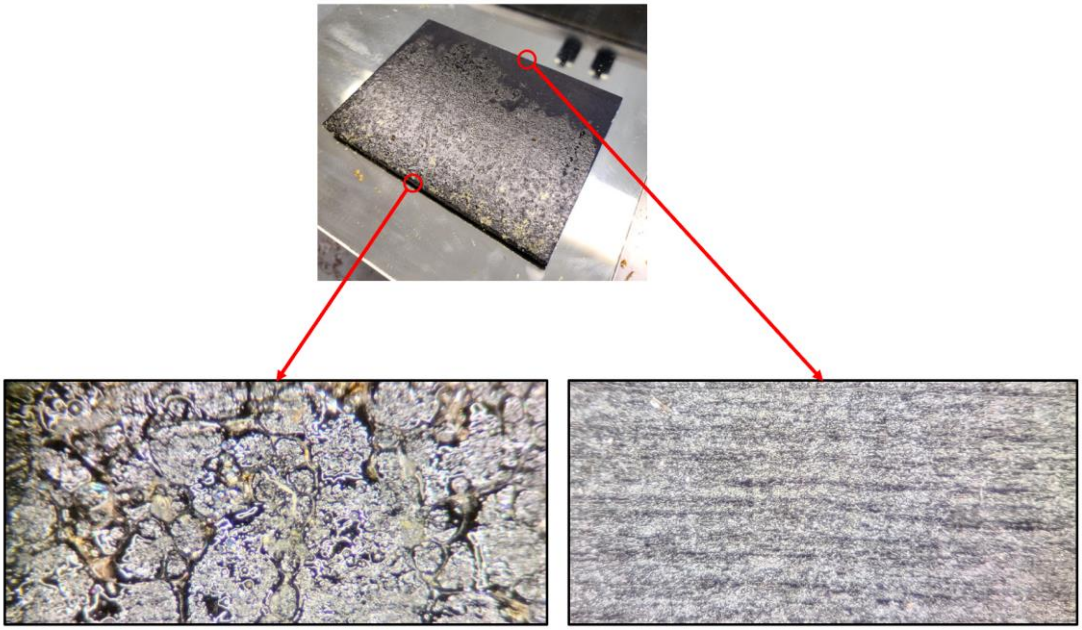

a b

Figure 5.1 Optical Microscopy of the Front and Back Edges of a Low-Pressure Re-Infiltrated Sample a) Front Edge of Sample b) Back Edge of Sample

These images seem to suggest that there may be an inconsistency in the amount of resin being deposited at different locations in the sample. This is further analyzed with SEM images, seen in Section 5.2

5.2. SCANNING ELECTRON MICROSCOPY

Scanning Electron Microscopy (SEM) was used in order to look closer at the microstructure of the samples. Samples were prepared in order to investigate the consistency of the matrix density throughout the sample. First, due to the inconsistent surface finish on the re-infiltrated samples, the resin density through the thickness of the sample. The following images were taken with a TM-1000 scanning electron microscope, at 15kV accelerating voltage and at various magnitudes. The samples were fractured prior to mounting into the SEM, in order to expose the inner surfaces of the sample. The samples were not coated or polished, in order to prevent resin shmearing into pores in the sample. Images were taken looking at various locations throughout the thickness of the sample, to verify consistent resin density. These images are shown in Figure 5.2.

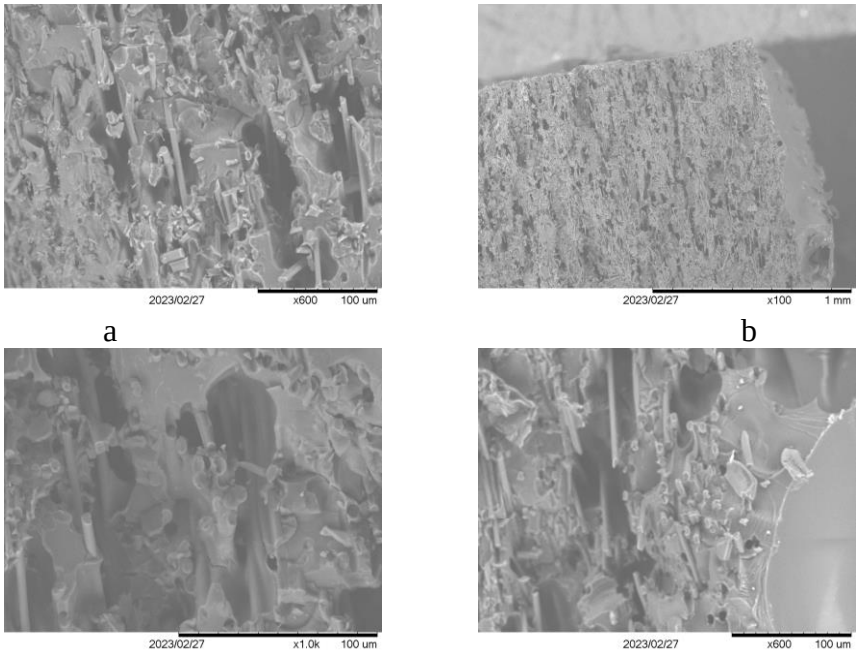

a b c d

Figure 5.2 SEM Images of Re-Infiltrated Samples, Various locations Through Thickness a) Center of Sample (x600) b) Edge of Sample (x100) c) Center of Sample (x1000) d) Edge of Sample (x600)

Looking at the above images, it does not seem that there is a considerable difference in the amount of resin deposited into the center of the sample versus the edge of the sample during re-infiltration. However, there does seem to be a solid coat of resin on the outside face of the sample, likely due to resin squeezing between the sample and the vacuum bag material during the infiltration process. This coat of resin explains the different surface finish present at varying locations across the surface of the re-infiltrated sample.

After verifying that resin was consistent throughout the entire thickness of the sample, further investigation into the inconsistent surface finish was performed. Six samples were taken from varying locations of the re-infiltrated sample, as seen in Figure 5.3. The SEM images are shown in Figure 5.4. The goal of these images is to determine if the matrix density is consistent at different locations in the sample, and to confirm that the resin is successfully infiltrating into the center of the sample, not just near the edges.

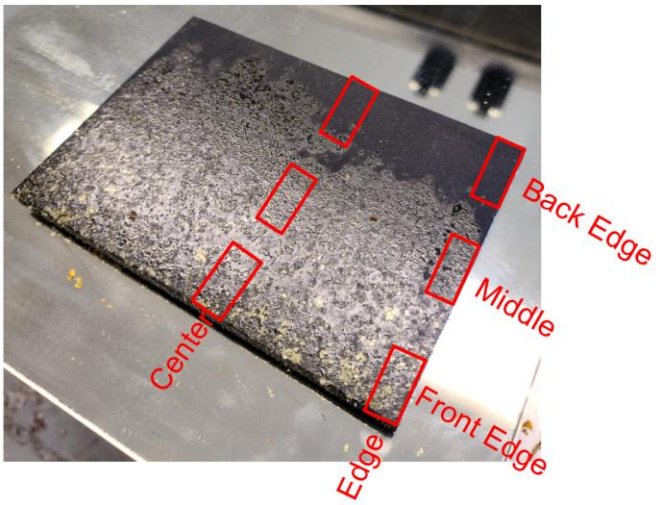

Figure 5.3 Sample Matrix for SEM Analysis

Looking at the images, there does not seem to be a clear inconsistency in the amount of resin deposited into the sample during re-infiltration. While there is a relatively high amount of porosity present in these samples, the amount and characteristics of the porosity remains constant throughout the images. These images suggest that the inconsistent surface finish present on the re-infiltrated samples did not have an effect on the amount of resin actually deposited into the sample.

Each of the sets of SEM images looked at a different question in the process in polymer re-infiltration. The analysis in each of these cases shows favorable results for this process, suggesting significant and consistent resin infiltration into additively manufactured composite samples after re-infiltration. As the process continues, SEM images will be taken in order to further verify these results, and to better understand the process of polymer infiltration and pyrolysis using a high-pressure re-infiltration process.

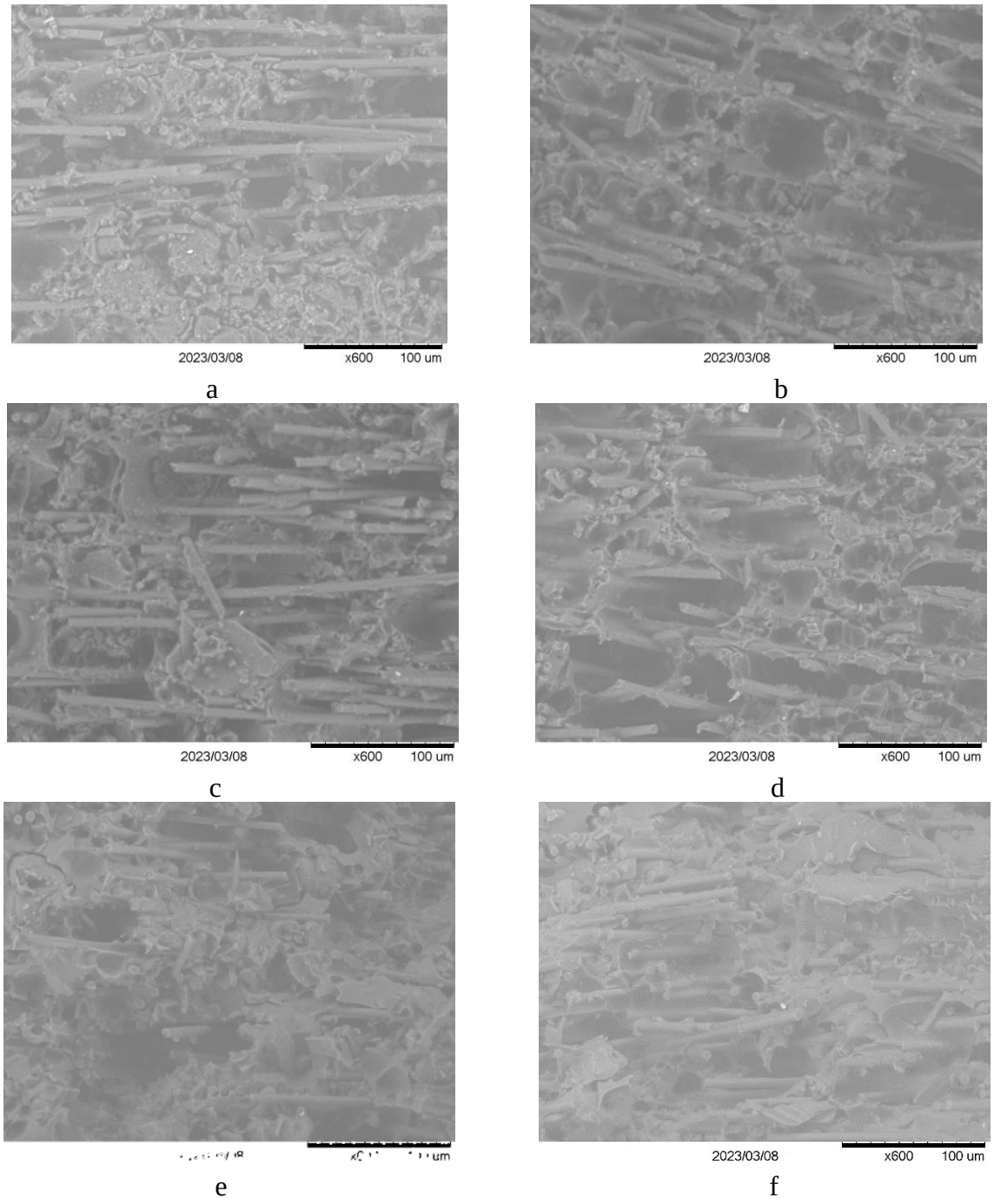

Figure 5.4 SEM Images of Re-Infiltrated Samples, Various Locations a) Front Edge, Center b) Front Edge, Edge c) Middle, Center d) Middle, Edge e) Back Edge, Center, f) Back Edge, Edge

6. RESULTS AND DISCUSSION

6.1. POROSITY

Results from the porosity analysis performed in Section 4.1 are shown below. Table 6.1 corresponds with the low-pressure re-infiltration results, while Table 6.2 denotes the high-pressure results.

Table 6.1 Low-Pressure Porosity Results

	Percent Open Porosity	
Stage	**Sample 1**	**Sample 2**
As Printed[1]	26.42	26.42
After 1st Pyrolysis	60.23	64.28
After 1st Re-Infiltration	16.22	36.51
After 2nd Pyrolysis	52.87	46.61

Between the 1st and 2nd pyrolysis cycles, there was a 12.22% and 27.36% decrease in the amount of open porosity present in the sample. This decrease in porosity corresponds to added carbon matrix material, converted during pyrolysis. This method is viable for creating a carbon/carbon composite; however, it would take many re-infiltration and pyrolysis cycles to create a dense part.

[1] Denotes results from acid digestion testing according to ASTM D3171-22.

Table 6.2 High-Pressure Porosity Results

	Percent Open Porosity
Stage	**Sample 3**
As Printed[2]	26.42
After 1st Pyrolysis	64.28
After 1st Re-Infiltration	2.31
After 2nd Pyrolysis	35.88

The re-infiltration cycle detailed above corresponds to a resin pressure of 1000psi. The high-pressure re-infiltration process is far more successful in filling the porosity within the sample with phenolic resin. Comparing the low-pressure and high-pressure results, the high-pressure system filled 24% more porosity than the low-pressure system. This increased resin corresponds to less porosity after the 2nd pyrolysis cycle as well. After the 2nd pyrolysis stage, the porosity was reduced by 44.18%. This difference corresponds with carbon matrix being deposited into the sample, successfully making a carbon/carbon composite.

6.2. MICROSTRUCTURE

Looking again at the SEM images in Figure 5.4, some qualitative results can be drawn. While the apparent porosity is high, much of the porosity is open, connected porosity. Open porosity is beneficial over closed porosity as open porosity remains

[2] Denotes results from acid digestion testing according to ASTM D3171-22.

accessible to resin for subsequent re-infiltration cycles. Cycles can be repeated, reducing the porosity each time until the desired porosity is reached. The SEM images also show a uniform distribution of porosity, suggesting that the part would possess more consistent properties.

7. CONCLUSIONS

This work suggests that a high-pressure polymer infiltration and pyrolysis technique is a viable method for producing dense ceramic matrix composite parts, faster than conventional techniques. Porosity analysis indicates that samples produced from the high-pressure technique possessed less latent porosity after re-infiltration than samples produced using low-pressure techniques. High-pressure samples had higher carbon matrix content after pyrolysis as well, suggesting a more effective CMC manufacturing technique. SEM analysis shows that much of the latent porosity is open porosity, which remains accessible to resin for further re-infiltration cycles. The high-pressure re-infiltration process developed for this work improved part quality while decreasing the processing time, reducing the time required to perform a re-infiltration cycle from weeks to hours.

8. FUTURE WORK

There is still a significant amount of work that can be done within this body of work. The high-pressure system developed in this work has a lot of potential for improvement. For example, adding a thermocouple and pressure transducer would allow for temperature and pressure data to be taken during re-infiltration and the curing process. Temperature data during the cure cycle would provide information on whether the mold is actually experiencing the temperatures dictated by the cure cycle, instead of relying on the oven temperature. Pressure data could be used to track the pressure throughout the cure cycle, to determine if pressure is held while the resin is curing, not just at the end of re-infiltration.

As mentioned in Section 3.4.3, the mold spacer can be tailored for different part geometries. Work could be done to investigate the effect of different mold shapes, in order to create a wider variety of parts. Shaped parts such as leading edges, nosecones, or turbine blades are of particular interest.

The aim of this work was to develop a process for high-pressure re-infiltration for composite parts, and this process can be applied to many different material systems. It would be possible to substitute a different matrix material, fiber, or both, in order to achieve different results. Examples include other pre-ceramic polymers, other polymers, and thermoset or thermoplastic resins. A variety of fibers could be used, such as glass or aramid fibers, and different forms, such as woven fiber mats or unidirectional fibers. One of the main advantages of this system is its high degree of customizability, for a variety of potential use cases.

After manufacturing samples, further testing could be done. Mechanical testing performed at room temperature and elevated temperature would provide information on the mechanical behavior of these composites at the temperature they are used at. Rather than performing Archimedes method for determining open porosity, computerized tomography (CT) scanning could be utilized to determine total porosity present in a sample after pyrolysis, including both open and closed porosity.

Finally, the porosity model presented in Section 4.2 could be verified with more testing. Expanding upon this model could provide the basis for numerical study of high-pressure re-infiltration, with simulations in place of actually manufacturing the parts. This would allow for faster and cheaper iteration of the process parameters.

BIBLIOGRAPHY

[1] Smith, C., Morscher, G., &; Xia, Z. (2008). Monitoring damage accumulation in ceramic matrix composites using electrical resistivity. *Scripta Materialia*, *59*(4), 463–466. https://doi.org/10.1016/j.scriptamat.2008.04.033

[2] Brosius D, “Boeing 787 Update”, High Performance Composites, May 2007

[3] Low, I.-M., &; Zhang, C. (2014). Understanding the wear and tribological properties of ceramic matrix composites. In *Advances in Ceramic Matrix Composites* (pp. 312–339). Woodhead Pub.

[4] Krenkel, W., & Naslain, R. (2008). In *Ceramic matrix composites: Fiber reinforced ceramics and their applications*. foreword, Wiley-VCH.

[5] Heimann, R. B. (2010). Preface. *Classic and Advanced Ceramics: From Fundamentals to Applications*. Wiley-VCH, https://doi.org/10.1002/9783527630172

[6] *The Advantage of Advanced Ceramics*. Ceramaret. (n.d.). Retrieved March 28, 2023, from https://ceramaret.com/en/advanced-ceramic-materials/the-advantages-of-advanced-ceramics

[7] Jacobson, N., Opila, E., & Lee, K. (2001). Oxidation and corrosion of ceramics and ceramic matrix composites. *Current Opinion in Solid State and Materials Science*, *5*(4), 301–309. https://doi.org/10.1016/s1359-0286(01)00009-2

[8] Mutin, P. H., & Boury, B. (2002). Ceramics, Chemical Processing of. In *Encyclopedia of Physical Science and Technology* (Third, pp. 621–636). Academic Press.

[9] Santhosh, U., Ahmad, J., Ojard, G., Smyth, I., Gowayed, Y., & Jefferson, G. (2020). Effect of porosity on the nonlinear and time-dependent behavior of ceramic matrix composites. *Composites Part B: Engineering*, *184*. https://doi.org/10.1016/j.compositesb.2019.107658

[10] Wang, X., Schmidt, F., Hanaor, D., Kamm, P., Li, S., & Gurlo, A. (2019). Additive manufacturing of ceramics from preceramic polymers: A versatile stereolithographic approach assisted by thiol-ene click chemistry. *Additive Manufacturing*, *27*, 80–90. https://doi.org/10.1016/j.addma.2019.02.012

[11] Dhanasekar, S., Ganesan, A., Rani, T., Vinjamuri, V., Nageswara Rao, M., Shankar, E., Dharamvir, Kumar, P., & Misganaw Golie, W. (2022). A comprehensive study of ceramic matrix composites for space applications. *Advances in Materials Science and Engineering*, *2022*. https://doi.org/10.1155/2022/6160591

[12] Nicholas, J., Meindes, R., Chandrashekhara, K., Hilmas, G., & Giraldo, C. (2014). Polymer Infiltration and Pyrolysis fabrication of SiC/SiC composite for nuclear applications. *CAMX 2014*.

[13] Schellhase, K., Koo, J., Buffy, J., & Brushaber, R. (2016). Development of new thermal protection systems based on silica/polysiloxane composites. *SAMPE*. https://doi.org/10.2514/6.2017-1367

[14] Li, J., Durandet, Y., Huang, X., Sun, G., & Ruan, D. (2022). Additively manufactured fiber-reinforced composites: A review of mechanical behavior and opportunities. *Journal of Materials Science & Technology*, *119*, 219–244. https://doi.org/10.1016/j.jmst.2021.11.063

[15] Wang, W., Bai, X., Zhang, L., Jing, S., Shen, C., & He, R. (2022). Additive Manufacturing of CSF/sic composites with high fiber content by direct ink writing and liquid silicon infiltration. *Ceramics International*, *48*(3), 3895–3903. https://doi.org/10.1016/j.ceramint.2021.10.176

[16] Packirisamy, S., Sreejith, K., Devapal, D., & Swaminathan, B. (2020). Polymer-derived ceramics and their space applications. *Handbook of Advanced Ceramics and Composites*, 975–1080. https://doi.org/10.1007/978-3-030-16347-1_31

[17] Shi, Y., Wan, Y., Zhai, Y., Liu, R., Meng, Y., Tu, B., & Zhao, D. (2007). Ordered mesoporous SIOC and SICN ceramics from atmosphere-assisted in situ transformation. *Chemistry of Materials*, *19*(7), 1761–1771. https://doi.org/10.1021/cm070283v

[18] Pilato, L. (2013). Phenolic resins: 100years and still going strong. *Reactive and Functional Polymers*, *73*(2), 270–277. https://doi.org/10.1016/j.reactfunctpolym.2012.07.008

[19] Hu, H., Wang, W., Jiang, L., Liu, L., Zhang, Y., Yang, Y., & Wang, J. (2022). Curing mechanism of Resole phenolic resin based on variable temperature FTIR spectra and thermogravimetry-mass spectrometry. *Polymers and Polymer Composites*, *30*. https://doi.org/10.1177/09673911221102114

[20] Hexion, Technical Data Sheet, Durite Resin SC-1008

[21] *The printer*. Impossible Objects. (2022, November 11). Retrieved March 29, 2023, from https://www.impossible-objects.com/cbam-printer/

[22] *Materials*. Impossible Objects. (2023, February 22). Retrieved March 29, 2023, from https://www.impossible-objects.com/materials/

[23] W. H. Li, A. Wong and D. Leach, “Advances in Benzoxazane Resins for Aerospace Applicatioins,” Proceedings of the 55th International SAMPE Technical Conference, 17 – 20 May 2010, Seattle, WA, pp. 1 – 9.

[24] Menta, V. G. K., Sundararaman, S., Chandrashekhara, K., Phan, N., and Nguyen, T., "Hybrid Composites using Out-of-Autoclave Process for Aerospace Sub-structures," *SAMPE International Symposium*, 53 (2008): 1-11.

[25] McNaught, A. D., & Wilkinson, A. (2000). Pyrolysis. In *IUPAC Compendium of Chemical Terminology* (p. 1824). Royal Society of Chemistry.

[26] Trick, K. A., & Saliba, T. E. (1995). Mechanisms of the pyrolysis of phenolic resin in a carbon/phenolic composite. *Carbon*, *33*(11), 1509–1515. https://doi.org/10.1016/0008-6223(95)00092-r

[27] Menta, V., Vuppalapati, R., Chandrashekhara, K., Schuman, T., & Sha, J. (2013a). Elevated-temperature vacuum-assisted resin transfer molding process for High Performance Aerospace Composites. *Polymer International*, *62*(10), 1465–1476. https://doi.org/10.1002/pi.4444

[28] X. Song, (2003). *Vacuum Assisted Resin Transfer Molding (VARTM): Model Development and Verification*, Blacksburg, VA. doi:10.4028/www.scientific.net/ddf.365.88

VITA

Samuel Brandt Weiler was born in Columbia, MO to Brian and Melanie Weiler on August 2, 1999. He received his Bachelors of Science in Aerospace Engineering from the Missouri University of Science and Technology in May of 2022. He joined the Master of Science degree program in Mechanical Engineering the following semester and in July of 2023 he received his M.S. degree in Mechanical Engineering from Missouri University of Science and Technology.